Postprint of: Jakóbczyk P., Kowalski M., Brodowski M., Dettlaff A., Dec B., Nidzworski D., Ryl J., Ossowski T., Bogdanowicz R., Low-power microwave-induced fabrication of functionalised few-layer black phosphorus electrodes: A novel route towards Haemophilus Influenzae pathogen biosensing devices, APPLIED SURFACE SCIENCE, Vol. 539 (2021), 148286, DOI: 10.1016/j.apsusc.2020.148286

Low-Power Microwave-Induced Fabrication of Functionalised Few-Layer Black Phosphorus Electrodes: A Novel Route Towards Haemophilus Influenzae Pathogen Biosensing Devices

Paweł Jakóbczyk[1*], Marcin Kowalski[1], Mateusz Brodowski[1], Anna Dettlaff[1,2], Bartłomiej Dec[1], Dawid Nidzworski[3,4,5], Jacek Ryl[6], Tadeusz Ossowski[7] and Robert Bogdanowicz[1]

[1] *Department of Metrology and Optoelectronics, Faculty of Electronics, Telecommunications and Informatics, Gdańsk University of Technology, Gabriela Narutowicza 11/12, 80-233 Gdańsk, Poland*

[2] *Department of Energy Conversion and Storage, Faculty of Chemistry, Gdańsk University of Technology, Gabriela Narutowicza 11/12, 80-233 Gdańsk, Poland*

[3] *Institute of Biotechnology and Molecular Medicine, 3 Trzy Lipy St., 80-172 Gdańsk, Poland*

[4] *SensDx, 14b Postępu St., 02-676 Warszawa, Poland*

[5] *Department of Recombinant Vaccine, Intercollegiate Faculty of Biotechnology, University of Gdansk and Medical University of Gdansk, Kladki 24, 80-822Gdansk, Poland*

[6] *Department of Electrochemistry, Corrosion and Material Engineering, Faculty of Chemistry, Gdańsk University of Technology, Gabriela Narutowicza 11/12, 80-233 Gdańsk, Poland*

[7] *Department of Analytical Chemistry, Faculty of Chemistry, University of Gdansk, 63 Wita Stwosza St., 80-952 Gdańsk, Poland*

[*] *corresponding author, pawel.jakobczyk@pg.edu.pl (Paweł Jakóbczyk), Phone: +48 58 347 19 76*

Abstract

In this paper, various passivation schemes were applied at few-layer black phosphorus (FLBP) to achieve covalent functionalisation with 4-azidobenzoic acid, improving its electrochemical response intended for analytical and biosensing applications. The thermal and microwave assisted modification procedures in toluene and dimethylformamide resulted in high reversibility of reactions on functionalised FLBP using a ferricyanide/ferrocyanide redox probe.

The lowest peak-to-peak separation of 91 mV, and high kinetics were obtained by thermal synthesis in dimethylformamide. Attachment of a =N-phenylene-COOH moiety to the FLBP limits its degradation under ambient conditions delivering a linker for a peptide bond with proteins in the $-NH_2$ groups.

The functionalised FLBP was applied for impedimetric detection of the Haemophilus Influenzae (HI) bacterial protein with a low limit of detection (LOD) of 5.82 $\mu g\ mL^{-1}$ along with high sensitivity equal to 1.267 $\%\ \mu g^{-1}$ mL. The proposed strategy delivers a novel phosphorene-based electrode for sensitive detection of various bacterial pathogens.

Keywords: black phosphorus electrodes, electrochemistry, microwave synthesis, pathogen detection, *Haemophilus Influenzae*

1. Introduction

Black phosphorus (BP) is the most stable allotrope of phosphorus in ambient conditions [1]. BP occurs in three crystalline configurations: rhombohedral, orthorhombic, and cubic systems [2,3]. A single, puckered layer of orthorhombic black phosphorus is called phosphorene. In the aforementioned form, each phosphorus atom has a lone pair of 3s electrons and is bonded

with three neighbouring P atoms by sp^3 hybridisation. The material belongs to the p-type semiconductor and is presently regarded as one of the most promising emerging 2D materials. Monolayer and few-layer BP can be used for high-performance device applications due to its tunable bandgap in the range of 0.3 eV to 2.0 eV, high hole mobility up to 10,000 $cm^2 V^{-1} s^{-1}$, anisotropic optoelectrical behaviour, high speed (cutoff frequency of 12 GHz), and good electron transfer conductivity [1,4–6]. However, nanosheets of black phosphorus exhibit high surface reactivity, whereby they show instability in ambient air conditions, which results in degradation of BP to various phosphorus acids [7–10] . Thus, layers of black phosphorus have not been used on a large scale yet.

Nowadays, there are several approaches to prevent oxidation of the BP surface, such as deposition of thick, inert poly(methyl methacrylate) (PMMA) films [11]. For this purpose, surfactants [12], perylenetetracarboxylic dianhydride (PTCDA) [13], polyvinylidene fluoride (PVDF) [14], and conducting polymers [15,16] are used. Moreover, BP layers can be embedded in Van der Waals heterostructures of graphene [17–20], carbon nanotubes [21], or MXenes [22,23]. It should be noted that all of these methods rely only on weak, non-covalent interactions. Alternatively, black phosphorus can be passivated using covalent functionalisation. There is a limited number of publications concerning such methods. Ryder *et al.* [24] modified a few-layer BP surface by a reaction with diazonium salt (4-nitrobenzene-diazonium and 4-methoxybenzenediazonium tetrafluoroborate salts) through the P-C bond. Sofer *et al.* [25], in turn, used nucleophilic reagents (alkyl halides, thionyl chloride, organolithium compounds). Covalent modification is also possible via the P=N double bond. Liu *et al.* grafted a benzoic acid group onto BP nanosheets [26]. There are several reports concerning density functional theory calculations of black phosphorus used as a biosensor [27–29], and a few papers concerning black phosphorus applied as a biosensor material. For this purpose, the black phosphorus is noncovalently modified by poly-L-lysine [30], nafion

[31], conducting polymer [32,33], hexamethylenediamine (HMA) [34], or polypeptide micelles [35]. However, due to the direct chemical bond, covalent functionalisation ensures better stability of the modified surface, and allows further modification of the material, which significantly extends the application possibilities.

We present four different procedures of covalent functionalisation of few-layer black phosphorus (FLBP) by reaction with 4-azidobenzoic acid. Covalent passivation by the attachment of the -N-Ar-COOH moiety onto FLBP protects it against degradation under ambient conditions. The carboxyl group -N-Ar-COOH could be applied as a linker with biological compounds, e.g., antibodies, due to the formation of a peptide bond with the $-NH_2$ group. Herein, we proposed a novel biosensing platform for *Haemophilus Influenzae* detection.

To the authors' best knowledge, this is the first time the covalently functionalised BP derivative material has been used as an electrochemical biosensor. Moreover, the thorough electrochemical characteristics and infrared spectroscopy analysis of the functionalised few-layer black phosphorus is also reported.

2. **Materials and methods**

2.1 Reagents

Black phosphorus (BP, >99.99%) was obtained from Smart Elements (Austria). Toluene (pure p.a.), potassium ferricyanide $K_3[Fe(CN)_6]$, sodium chloride (≥99%, anhydrous, ACS reagent), sodium sulfate (≥99%, anhydrous, ACS reagent), N, N-dimethylformamide (DMF, pure p.a.), and methanol (pure p.a.) were purchased from POCH (Poland). Glassy carbon in powder form (GC in powder, 99.95%), paraffin oil (meeting the analytical specification of Ph. Eur., BP), N-hydroxysuccinimide (NHS), 1-ethyl-3-(3-dimethylaminopropyl)-carbodiimide (EDC),

bovine serum albumin (BSA), and phosphate-buffered saline (PBS) were acquired from Sigma-Aldrich (USA). 4-azido-benzoic acid (≥97%, Germany) was attained from Carbosynth Limited (UK). All reagents were used as received from the suppliers.

2.2 Few-Layer Black Phosphorus (FLBP) preparation

Phosphorene (few-layer black phosphorus, FLBP) was prepared from pre-crushed black phosphorus (BP) (50–60 mg) dispersed in anhydrous dimethylformamide (7 mL) in an argon atmosphere. The process of liquid exfoliation was carried out in an ice bath, at a temperature from 0 to 3°C, under a stream of argon using a horn probe ultrasonicator (Bandelin Sonopuls HD2200, 20 kHz). The sonication power and time amplitudes were 40 W and 50/50, respectively. The sonication-aided exfoliation process took 120 min. Afterwards, the resultant suspension was centrifuged at 6000 rpm for 5 minutes to remove the residual unexfoliated particles, yielding supernatant. Next, exfoliation was repeated for the unexfoliated residue for another 2 h. After the finish, the centrifugation of reexfoliated suspension was repeated. The phosphorene with a concentration of 1 mg per solvent millilitre was used for the reaction. The preparation of phosphorene in toluene differed in the centrifugation step, where the centrifugation time was shortened to 3 min and a spin rate of 3000 rpm.

2.3 Synthesis of Functionalised Few-Layer Black Phosphorus (f-FLBP)

The reaction of FLBP with 4-azidobenzoic acid led to the formation of functionalised phosphorene (f-FLBP). Functionalisation was carried using microwaves (microwave method) or using high temperature (temperature method). The temperature method in DMF was the reconstructed method from the literature [36] with a change only in the reaction time from 48 h to 36 h. Table 1 presents the conditions of the reaction conducted.

Table 1. Parameters of carried out reactions f-FLBPs with 4-azidobenzoic acid

Reaction product symbol	Method	Solvent	Temperature / °C	Microwaves / W	Time / h
f-FLBP_DMF-T	Temperature	DMF	140	-	36
f-FLBP_tol-T	Temperature	toluene	140	-	36
f-FLBP_DMF-MW	Microwave	DMF	70	10	2
f-FLBP_tol-MW	Microwave	toluene	70	120	2

The reaction mixture was prepared as follows, the solution of FLBP in DMF or toluene with a concentration of 1 mg mL^{-1} and 4-azidobenzoic acid were mixed in an autoclave at a ratio of 5 to 32. The reaction mixture was deaerated by freezing three times in liquid nitrogen, evacuated and saturated with argon during heating up to the ambient temperature. The synthesis was carried out in conditions presented in Table 1. After that reaction product was three times centrifuged (10000 rpm) for 30 min, it was rinsed with methanol. In the next step, it was dried under reduced pressure for 24 h at 25 °C. In the case of a reaction in the presence of microwaves, it was carried out in a microwave synthesiser (Discover® SP). The different power levels used in the reactions results from the different solvents. In the case of DMF, the use of 120 W of power increased the temperature above 70 degrees Celsius and did not stabilise it. Therefore, the adapted reaction power was 10 W. In toluene, 120 W of microwave power was adequate to bring the reaction mixture to 70 degrees Celsius. In Figure 1, the route of FLBP functionalisation by reaction with 4-azidobenzoic acid to f-FLBP is shown.

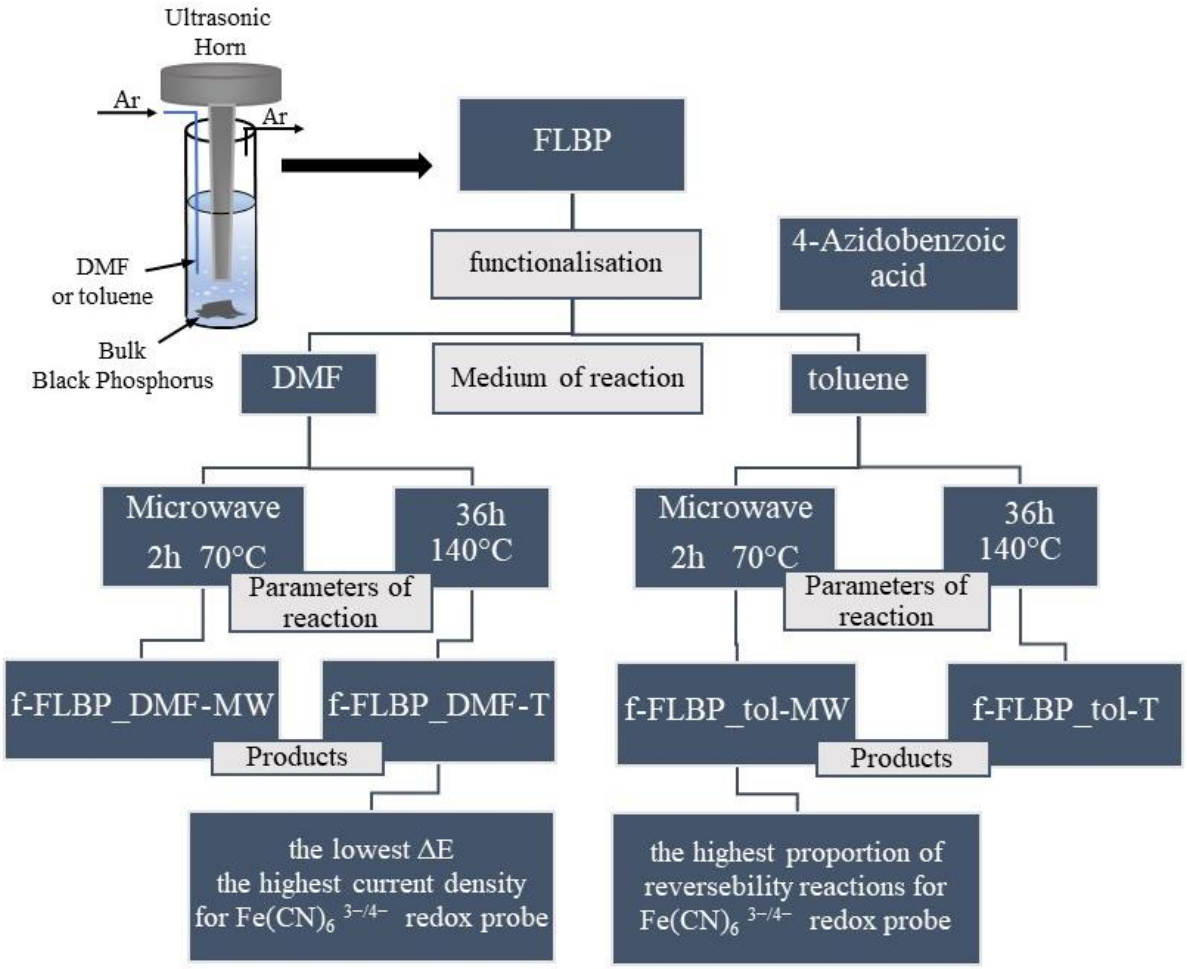

Figure 1. Scheme of the functionalisation of f-FLBP with 4-azidobenzoic acid

2.4 f-FLBP electrode preparation

Functionalised phosphorene electrodes were prepared with a composition of 10 wt% few-layer black phosphorus (FLBP), 20 wt% paraffin oil, and 70 wt% conductive material (glassy carbon in powder form) by mixing with toluene solvent. The suspension of solid components in toluene was cast on a 3 mm in diameter glassy carbon electrode. After solvent evaporation in an argon atmosphere and next in a vacuum, a layer of f-FLBP electrode was formed containing the active material (f-FLBP), electronic conductor (glassy carbon in powder form), and the binder (paraffin oil). The electrodes produced this way were used for electrochemical studies as well as for further modification to detect bacterial protein.

2.5 Computational method

Density Functional Theory (DFT) calculations were conducted with Quantum ATK code from Synopsys [37,38]. All computation was done with a General Gradient Approximation (GGA) with the Perdew-Burke-Ernzerhof exchange-correlation functional. For calculating electron properties, the Linear Combination of Atomic Orbitals technique was used. Such a method provided the possibility of calculating non-periodic structures. The designed structure was non-periodic in the z-direction and periodic in the x- and y-directions. Such a structure was done in accordance with Green's-function method for surface calculations [39]. At the cell boundary, with the phosphorene layers, the Dirichlet boundary condition was set. Next, the Neumann boundary condition was applied at the vacuum cell edge of the slab. In all configurations, k-points sampling was (4, 3, 90) with a 75 Hartree mesh cut-off. In all calculations, the Fritz-Haber Institute (FHI) pseudopotential code was utilised. The slab of the system was described as the simple orthorhombic lattice type. The size of the supercells was set to 6.6272 Å x 8.7526 Å x 40.0000 Å in the x,y,z directions for all configurations. The first configuration was a pristine surface constructed from phosphorene layers without any functionalisation. The slab was optimised and built with 64 phosphorus atoms. The two layers at left were repeated and used as an infinite electrode. The second and third system was made based on the first one, including a single- or double-bonded 4-azidobenzoic acid molecule (4-azidobenzoic acid) on the BP surface. The number of atoms in both systems increased to 79 atoms due to the 4-azidobenzoic acid modification.

2.6 Characterisation techniques of f-FLBP

The electrochemical studies involved cyclic voltammetry (CV). A Potentiostat-galvanostat (VMP-300, Bio-Logic, France) was employed. The f-FLBP layer was applied to the GC electrode inside an argon-filled glovebox (MBraun B200). All electrochemical tests of f-FLBP were carried out in a three-electrode system under an argon atmosphere. The f-FLBP

electrode was used as the working electrode and the Ag|AgCl|3.0 M KCl electrode and Pt wire were used as the reference and the counter-electrode, respectively. CV measurements were carried out in aqueous deoxygenated 1 mol dm^{-3} Na_2SO_4 and recorded a potential window in the range from -1 to 1V versus the Ag|AgCl|3.0 M KCl electrode for a scan rate equal to 20 mV s^{-1}. Cyclic voltammetry was also carried out in 5 mM $Fe(CN)_6^{3-/4-}$ in a 0.5 mol dm^{-3} Na_2SO_4 solution at 100 mV s^{-1}. During all electrochemical measurements, the electrochemical cell was kept in a Faraday cage to minimise the electrical noise. For the identification of the functionalisation products, the IR spectra were recorded with a Bruker IFS66 spectrometer using KBr pellets. XPS analysis was performed to determine changes in chemical composition of functionalized FLBP and to get information on the oxidation of the FLBPs and f-FLBPs surfaces. XPS measurements were conducted using Escalab 250Xi spectroscope (Thermo Fisher Scientific) with monochromatic Al X-ray source and a spot diameter od 200 μm. The morphology of the few-layer black phosphorus and its functionalization products were characterized by a scanning electron microscope (SEM) (Phenom XL, Thermo Fisher Scientific). A secondary electron detector with 10 kV beam accelerating voltage was used working in high vacuum mode pressure.

3. **Density functional theory calculations**

The combination of phosphorus with 4-azidobenzoic acid is a nucleophilic substitution reaction. As predicted by (density functional theory) DFT, simulations show that a single or double phosphorus nitrogen bond can be formed (Figure 2). Such behaviour was also shown in the literature [36], where it was confirmed that the combination of phosphorus with 4-azidobenzoic acid is a nucleophilic substitution reaction. Moreover, our study revealed that the double-bonded configuration is more energetically favourable and, therefore, more stable.

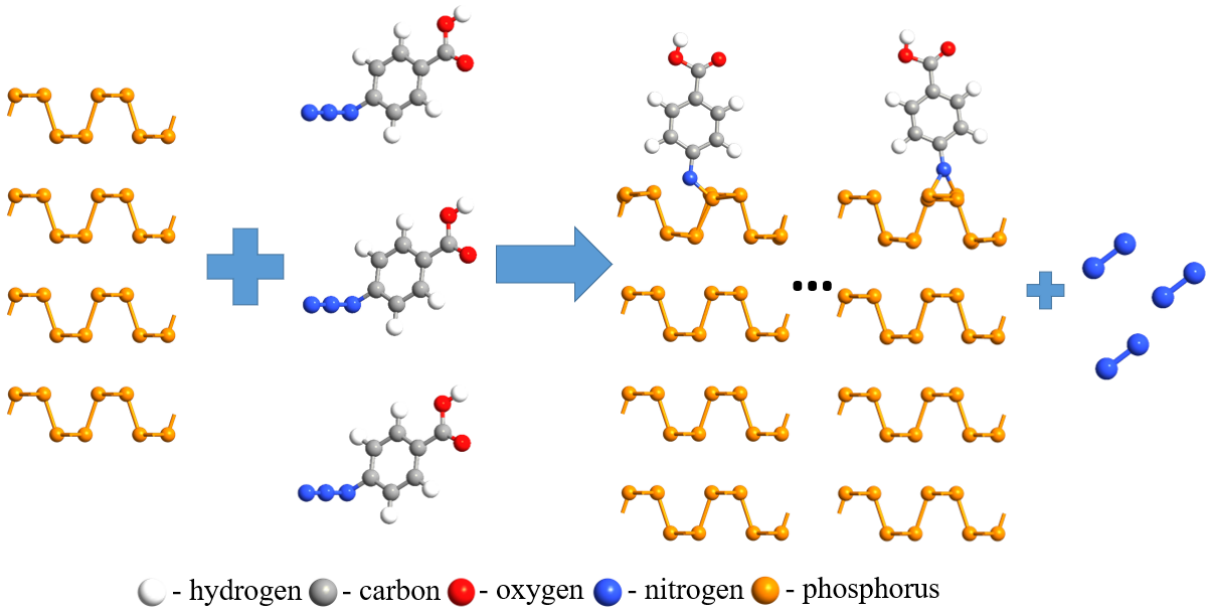

Figure 2. The proposed reaction of the surface of FLBP with 4-azidobenzoic acid.

The effective potential variations of the FLBP surface show that the electronegativity of the surface increases with the attached 4-azidobenzoic acid. Such behaviour suggests a higher affinity to reactions of the activated surface than bare FLBP (Supplementary Figure S1a, c). At the FLBP surface, there is also a higher electron density when 4-azidobenzoic acid is attached. This fact also indicates a higher efficiency of covalent bonding than for bare FLBP (see Figure S2). Furthermore, the study of surface electron properties showed behaviour dependent on the bonding configuration. A single bonded molecule disrupts the phosphorene layer by far more than the double-bonded configuration.

Additionally, the Projected Local Density of States (PLDOS) data showed that double-bonded 4-azidobenzoic acid induces a higher probability of empty electron states in the conduction region, which suggests that the electron flow from 4-azidobenzoic acid to the surface will be higher than in the single-bond configuration (Figure S4). The HOMO-LUMO gap is increased in the second configuration to 1.11 eV (Figure S3c). The single bonded configuration does not influence the bandgap value (Figure S3a).

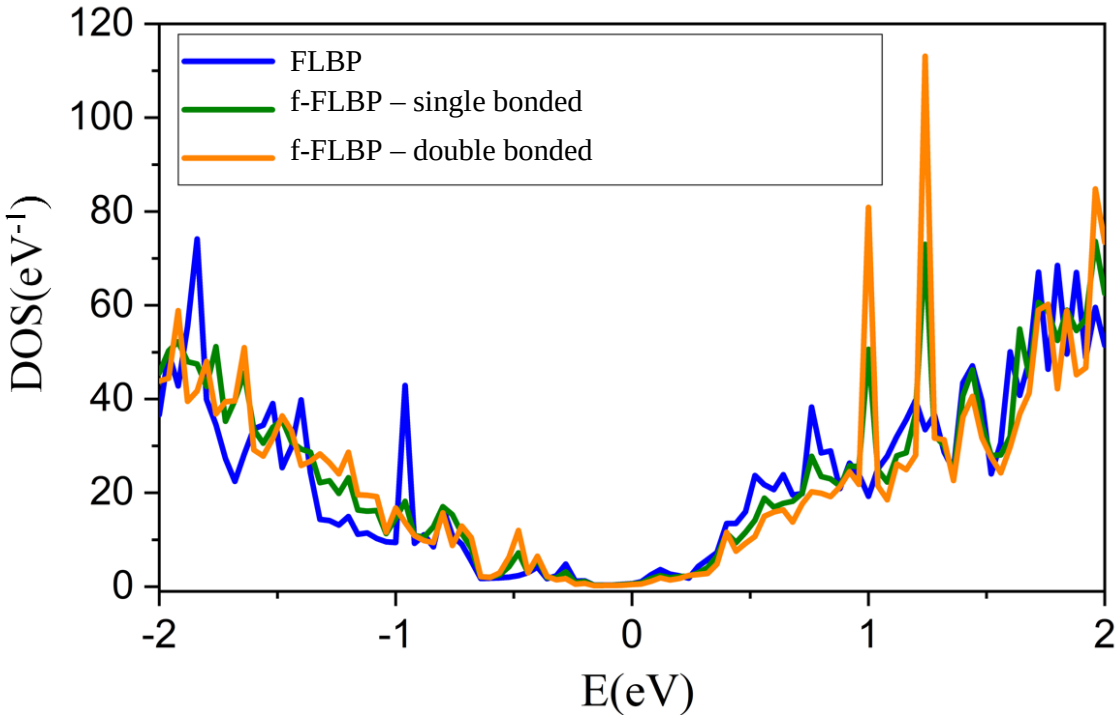

Figure 3. Density of States of FLBP surface with single and double bonded 4-azidobenzoic acid.

The localisation of electrons along different energy intervals influences the density-of-states diagram (Figure 3). The local variation of DOS illustrated in Figure S4 revealed large DOS amplitudes at the double-bonded linker. As a result of the reaction, the product which is created significantly affects the energy states (Figure 3). The surface with f-FLBP shows significant peaks in the conduction band at 1 eV and 1.25 eV, meaning that due to surface activation, we induced more unoccupied states. The semiconductor nature and the availability of free electrons in the conduction band make f-FLBP a suitable material for electrochemical sensors [40–42].

4-azidobenzoic acid reacts with few-layer black phosphorus. Thus, a double bond is formed between the nitrogen and the phosphorus surface, producing covalent passivation, which protects the FLBP against degradation [36], and provides the possibility of using this material as a platform for biosensors. Such an effect is attained thanks to the carboxyl group as a linker

with biological compounds, e.g., antibodies, which form a peptide bond with the amino group.

4. Results and discussion

4.1 Structure and morphology of functionalised Few-Layer Black Phosphorus

Infrared spectra confirm the conducted reaction by the proposed methods. Figure 4 shows the spectra of bare FLBP as well as 4-azidobenzoic acid. Fourier transform infrared spectroscopy (FTIR) analysis was performed in the mid-infrared spectrum (3800–400 cm^{-1}). The broad peak observed in the black phosphorus sample, and all composites at 3440 cm^{-1} is attributed to the -O-H stretching band, whereas H_2O is identified by a symmetrical band 1632 cm^{-1}[43], so it can be assumed that the chemisorption of water by few layered black phosphorus occurred during sample transfer to FTIR analysis [44]. Azidobenzoic acid shows the characteristic asymmetric stretching frequencies of the $-N_3$ moiety at 2106 cm^{-1} [45]. The peak is absent for the f-FLBP composites and FLBP, which suggests that there is no unreacted substrate. For f-FLBP_DMF-T, f-FLBP_tol-T, f-FLBP_DMF_MW, f-FLBP_tol_MW, and f-FLBP_DMF a transmittance peak was recorded at approximately 1170 cm^{-1} resulting from phosphorus oxidised during synthesis (P-O stretching) [46]. A strong, broad peak presented in 4-azidobenzoic acid in the range of 3000–2500 cm^{-1} is attributed to the -O-H stretching of the carboxylic group. The strongest signal originating from the -COOH moiety exhibits f-FLBP_tol_MW and then f-FLBP_tol-T. In this region, there are also overlapping signals at 2852 cm^{-1} and 2924 cm^{-1} resulting from -C-H stretching of sp^3 carbon. This acid moiety also produces signals at 1685 cm^{-1}, 1430 cm^{-1}, 1289 cm^{-1}, and 927 cm^{-1}, which can be attributed to C=O stretching, in-plane -O-H bending, C-O stretching, and out-of-plane -O-H bending bands [46]. There is a P=N functional group present at a frequency of ca. 1380–1390 cm^{-1}, which has been observed in the literature at about 1320 cm^{-1} [47], however, due to different adjacent groups, this binding has been shifted. The P=N signal is absent in f-FLBP_DMF_MW,

suggesting incomplete synthesis. In this range, there are transmittance peaks from the C=O group, which makes interpretation ambiguous. Analysis of the FTIR results revealed that except for the f-FLBP_DMF-MW composite, the synthesised f-FLBP_DMF-T, f-FLBP_tol-T, and f-FLBP_tol-MW samples were efficiently functionalised.

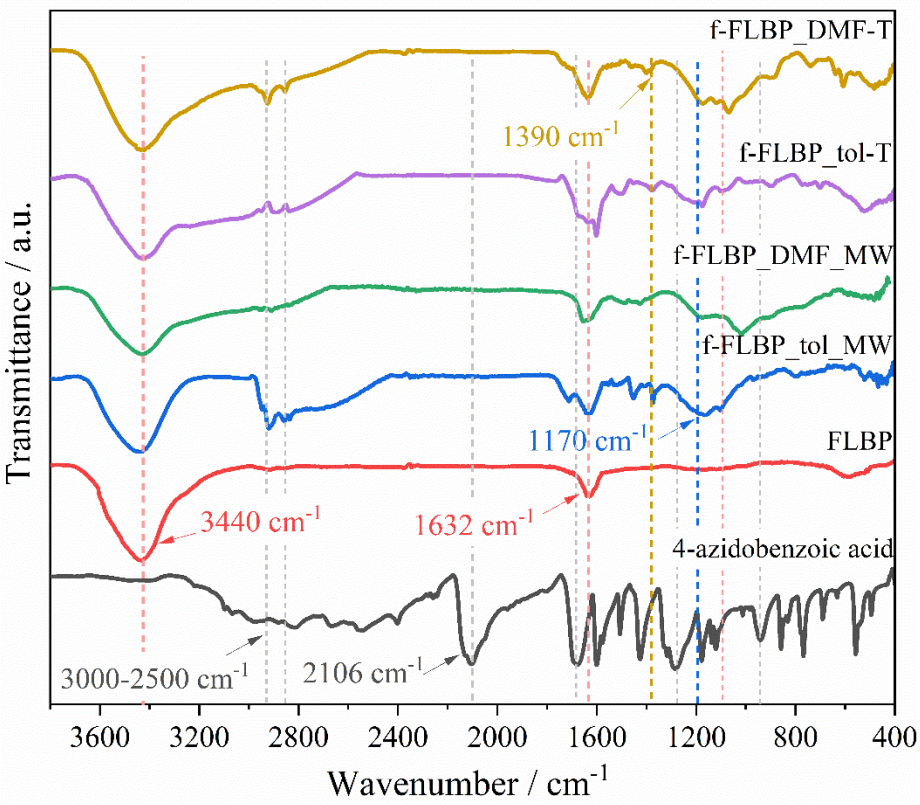

Figure 4. Infrared spectrum of f-FLBP_DMF-T, f-FLBP_tol-T, f-FLBP_DMF-MW, f-FLBP_tol-MW, FLBP and 4-azidobenzoic acid.

It should be emphasised that toluene is not the preferred solvent for the nucleophilic substitution reaction (S_N2), because it belongs to the group of nonpolar solvents. In S_N2 reactions, polar aprotic solvents are preferred, which tend to have high dipole moments, and do not have -OH and -NH moieties in their structures [48]. Thanks to the use of microwaves, the functionalisation reaction of FLBP by 4-azidobenzoic acid was efficiently carried out in toluene. The main advantage of this process is the uniform heating of the substrates. In the conventional method, the heat transfer is directly related to the extent of heat diffusion, i.e., heat transfer begins from the surface of the solution [49]. The capability of microwaves

(electromagnetic radiation) to engender uniform heating improves the interaction between the FLBP and 4-azidobenzoic acid. Microwaves only interact with polar molecules; thus toluene is inert in the reaction. The FTIR spectra of the f-FLBP_tol-MW reveal the largest separation of peaks.

The high-resolution XPS spectra recorded in P 2p core level (Fig. 6 a and b) manifest a predominant P-P peak doublet, with P $2p_{3/2}$ at 130.1 eV [50]. The modification in toluene leads to significantly hindered phosphorus contribution, due to the electrode surface coverage by 4-azidobenzoic acid and other compounds. For f-FLBP_tol-T, the P-P peaks are less distinctive but visible, while for f-FLBP_tol-MW the P-P contribution is negligible. The second P 2p spectral component, visible in each analyzed sample, lies in the binding energy range characteristic of P=N bonds (P $2p_{3/2}$ at approx. 133.3 eV [51], appearing as a result of bond formation between 4-azidobenzoic acid and FLBP [26]. It should be noted that P-OH bonds forming due to FLBP oxidation during functionalization would consequence in a peak doublet emerging in the same energy range. Thus, the successful P=N bond formation was confirmed with N 1s peak at 401.5 eV (N 1s spectra in the inset of Fig. 6 a, b) [51]. The presence of DMF decomposition products is visible also through a weak amine (C-N) bond in N 1s spectra with core energy level of 399.4 eV [52]. Importantly, the discussed anchoring of 4-azidobenzoic acid to FLBP appears to be the strongest for f-FLBP synthesized at higher temperatures and without the use of microwaves.

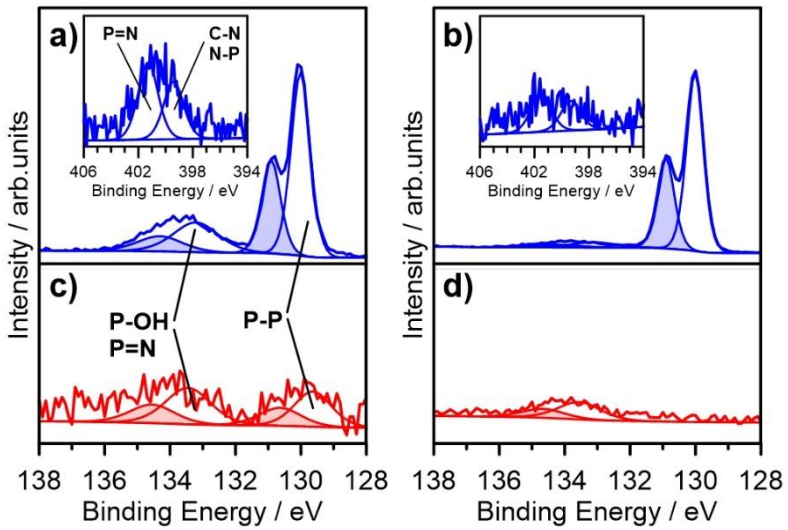

Figure 6. The high-resolution P 2p XPS spectra of functionalised few-layer black phosphorus: (a) f-FLBP_DMF_T, (b) f-FLBP_DMF-MW, (c) f-FLBP_tol-T, (d) f-FLBP_tol-MW.

Scanning electron microscopy (SEM) was used to investigate the morphology of FLBP and functionalisation products of FLBP. Fig. 7 E presents typical SEM image of bare FLBP, the surface consist of flakes in the size of a few micrometers, disordered with each other with their boundaries clearly marked. In the remaining images (7 A-D), the f-FLBP flakes are less visible, agglomerate together, their less visible structure proves their coverage by other compounds. This is especially visible in Figure 7 D, where the surface is relatively flat and smooth which might indicate that a coveraged is the thickest.

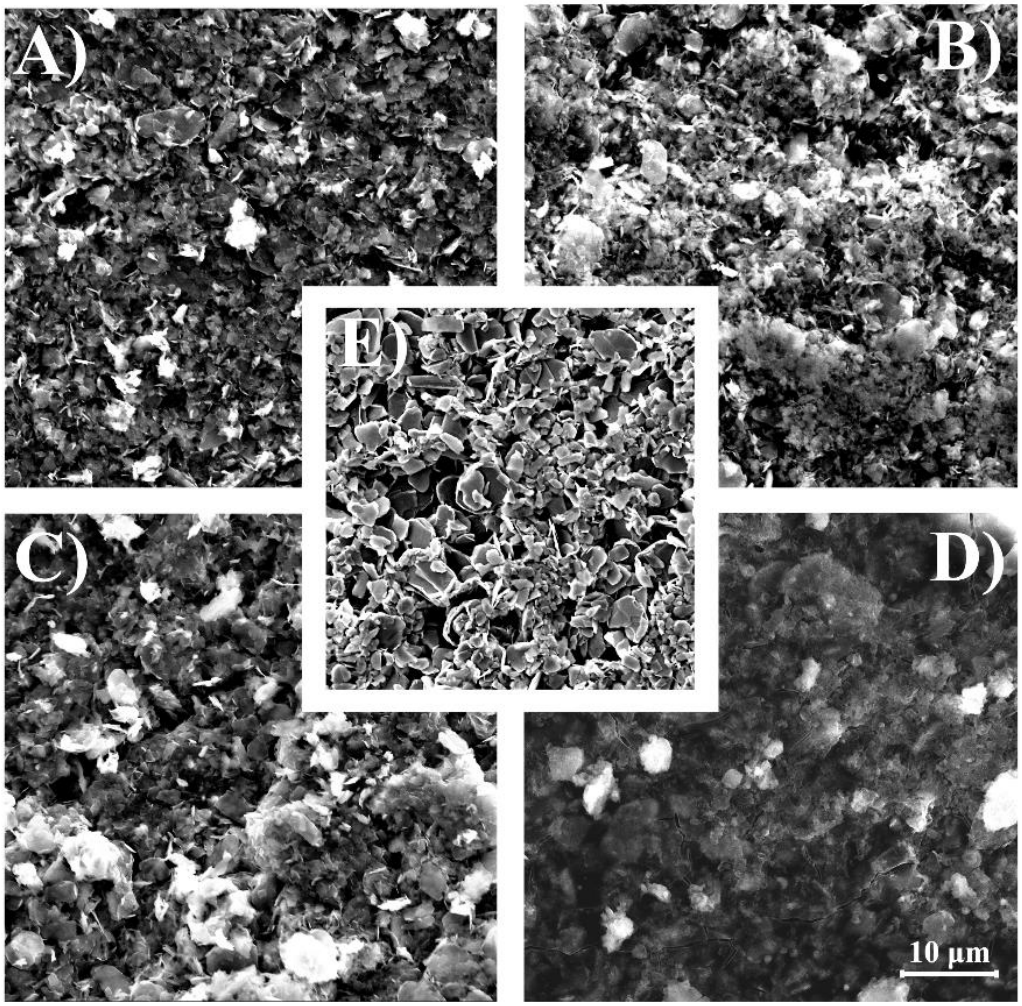

Figure 7 SEM images of: (A) f-FLBP_DMF-MW, (B) f-FLBP_tol-MW, (C) f_FLBP_DMF-T, (D)f f_FLBP_tol-T, (E) FLBP, at a magnification of 5000×.

4.2 Cyclic voltammetry of f-FLBPs

Cyclic voltammetry (CV) was used to determine the electrochemical performance of f-FLBPs. The obtained CV results show that the FLBP surface is electrochemically active and undergoes an irreversible oxidation process (Figure 8). According to the literature [53,54] , the peak recorded at a potential of about 0.6 V (*vs.* Ag|AgCl|3M KCl) is associated with the electrochemical oxidation of elemental phosphorus P(0) to the fifth oxidation state forming phosphate ions (PO_4^{3-}). The prior materials (FLBP) obtained in DMF (FLBP_DMF) and in toluene (FLBP_tol) recorded various shapes of cyclic voltammetry curves [36]. It was noticed that FLBP_DMF delivers much higher current densities in 1M Na_2SO_4, (Figure 8a, c; 2 mA

cm^{-2}) than FLBP_tol, which results in a current density in the order of 10^{-5} mA cm^{-2} (Figure 8b, d) at a scan rate of 20 mV s^{-1}. This phenomenon is attributed to the surface area of FLBP and the moiety attachment to the surface of FLBP, which is different to what few-layer black phosphorus produces in DMF and toluene [55]. The large specific surface area of FLBP and the presence of hydroxyl groups contribute to the transmission of larger quantities of electrons and enhanced current density response [34].

The f-FLBP_DMF-T (Figure 8a) and f-FLBP_tol-MW (Figure 8d) revealed strongly pronounced phosphorus oxidation peaks at about 0.6 V [53]. The oxidation density current for this peak reaches 3 mA·cm^{-2}. This indicates that the FLBP surface is not fully functionalised by 4-azidobenzoic acid. Thus, the phosphorus oxidation peak disappears after the first cycle of CV [54]. The presence of the oxidation peak at a potential of approx. 0.3 V for f-FLBP_DMF-T and f-FLBP_tol-T during cyclic voltammetry (Fig. 7 a, b) indicates additional functional groups at the surface of functionalised FLBP. This peak is not present for the f-FLBPs obtained in microwaves. A reactive reagent like as 4-azidobenzoic acid could decompose in higher temperature and react with surface of FLBP [56]. The oxidation peak may be related to the oxidation of the obtained phosphorus-nitrogen moieties at the surface of FLBP [57]. In the case of f-FLBP_tol-MW, gradually decreasing oxidation peaks in the subsequent sweep cycles from -1 to 1 V potential (Figure 7d) were recorded, which may be associated with a larger surface area of bare FLBP than on f-FLBP_DMF_T surfaces [31]. The f-FLBP_tol_T (Figure 8b) showed the lowest current density response, and hence, the lowest electron transfer rate. The peak from phosphorus oxidation is weak in the first cycle, and is absent in the subsequent cycles. As mentioned above, toluene is not an appropriate solvent in a typical S_N2 reaction, hence the lowest degree of phosphorene conversion, and thus the lowest functionalised surface of f-FLBP_tol-T takes form a place during reaction in

toluene solvent. This results in the highest resistance of the f-FLBP_tol_T electrode surface during interphase electron exchange.

The highest anode current density during the CV measurement occurs for the f-FLBP_DMF-MW (Figure 8c), while the oxidation peak of phosphorus is invisible. The oxidation peak is broad due to high resistance of electrode. An effective polar solvent, DMF is not only solvent but also reagent participating, thanks to its structure, in various reactions. The interaction of DMF decomposition products in microwave reactor with surface of FLBP is complex process [58]. The high peak of oxidation in 1 M Na_2SO_4 (Fig. 8c) is associated with the oxidation of DMF decomposition products [59].

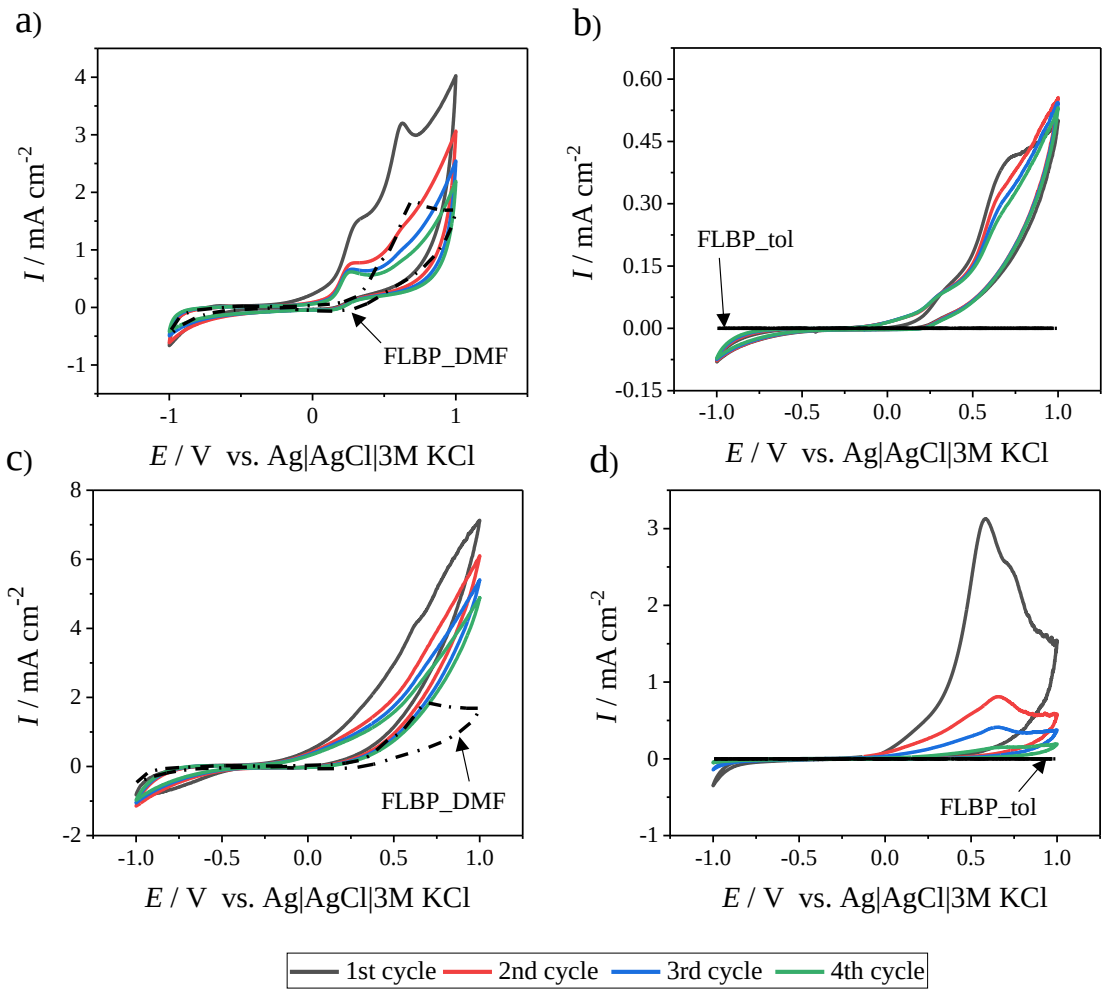

Figure 8. Cyclic voltammograms of FLBP (prepared in DMF (FLBP_DMF) and in toluene (FLBP_tol)), and functionalised FLBP: (a) f-FLBP_DMF-T; (b) f-FLBP_tol-T; (c) f-FLBP_DMF-MW;(d) f-FLBP_tol-MW in 1 M Na_2SO_4. Scan rate, 20 mV s^{-1}.

Cyclic voltammetry was carried out in 5 mM $Fe(CN)_6^{3-/4-}$ in a 0.5 mol dm^{-3} Na_2SO_4 solution at 100 mV s^{-1} (Figure 9). A hexacyanoferrate(II)/hexacyanoferrate(III) redox couple was used to test the electron transfer properties of the f-FLBPs [60,61]. The obtained CV curves show the highest oxidation current density values for f-FLBP_DMF_MW (Figure 9c), where the oxidation peak is similar to that in Fig. 9 c and a wave broadening is visible, due to higher resistance of f-FLBP_DMW-MW than for f-FLBP_DMF-T and f-FLBP_tol-MW [62,63]. A wave broadening is seen besides in Fig. 9 b.

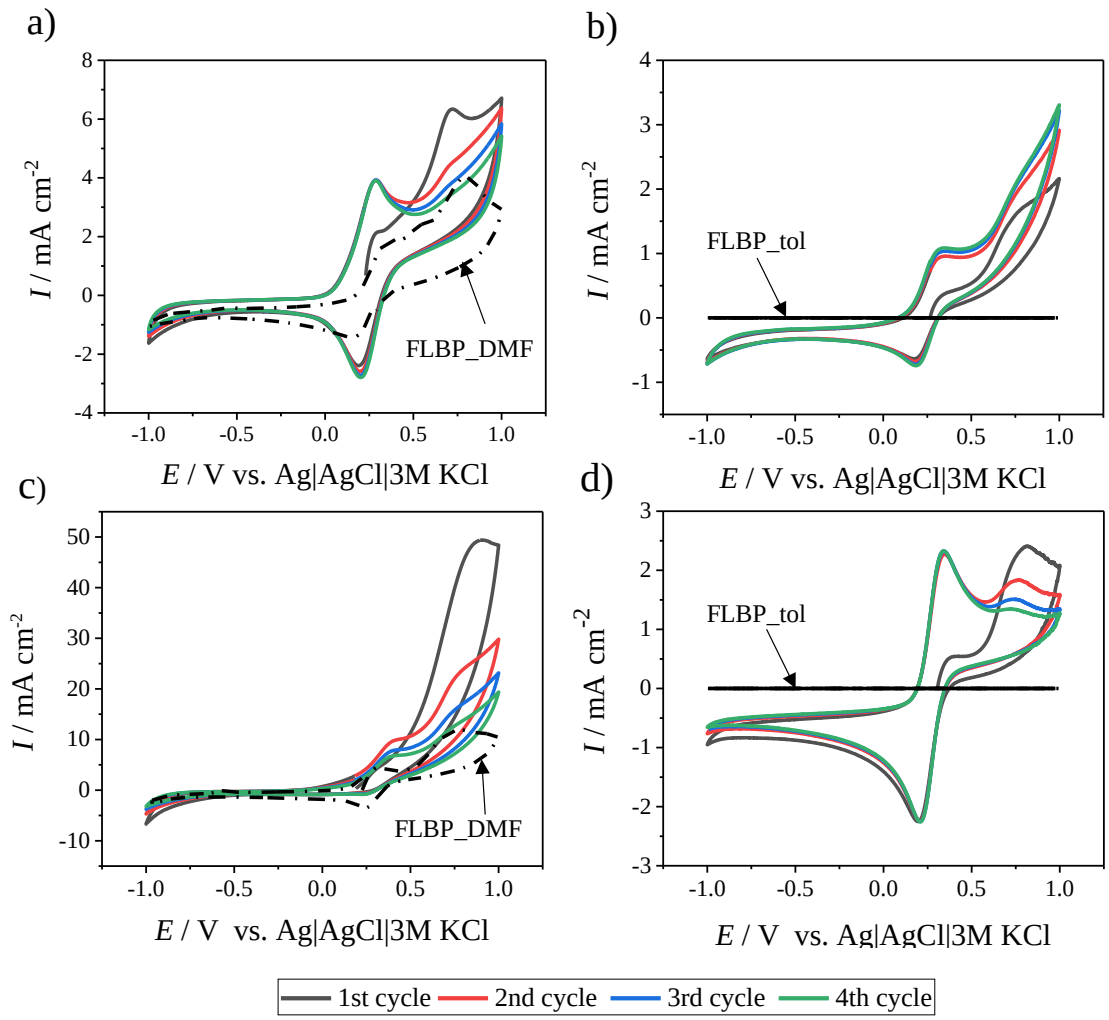

Figure 9. Current density values as a function of the potential recorded at 100 mV s^{-1} in contact with redox electrolyte 5 mM $K_3[Fe(CN)_6]$/0.5 M Na_2SO_4 recorded for phosphorene (prepared in DMF (FLBP_DMF) and in toluene (FLBP_tol)) and functionalised phosphorene: (a) f-FLBP_DMF-T; (b) f-FLBP_tol-T; (c) f-FLBP_DMF-MW; (d) f-FLBP_tol-MW.

The average data of all recorded samples with the error expressed as standard deviation (S) were shown in Table 2. The highest density currents for redox reactions were observed for f-FLBP_DMF-T. The peak-to-peak separation (ΔE) of f-FLBP_DMF-T equals only 91 mV (Table 2). This indicates that f-FLBP_DMF-T possesses the highest required surface performance to provide rapid electron transfer for the ferricyanide/ferrocyanide redox system and the lowest resistance of functionalised surface [64,65]. The f-FLBP_tol_MW, as an electrode material, displays symmetric of anodic and cathodic relations, which points at a smallest amount of side reaction of functionalization at the surface of f-FLBP [61]. The difference in potential between the oxidation and reduction peaks of f-FLBP_tol-MW reaches 147 mV, and is similar to the f-FLBP_tol-T electrode, where the peak separation amounts to 154 mV (Table 2). The f-FLBP_DMF-MW electrode reveals improved EC performance versus the initial FLBP obtained in DMF. Unfortunately, the FLBP_tol surface does not exhibit both electrochemical activity and redox reactions [66].

Table 2. Electrochemical parameters of FLBPs and f-FLBPs estimated from cyclic voltammetry

Functionalised phosphorene symbol	$I_{peak(ox)}$ / **mA cm^{-2}**	±**S** / **mA cm^{-2}**	$I_{peak(red)}$ / **mA cm^{-2}**	±**S** / **mA cm^{-2}**	Δ***E*** / **mV**	±**S** / **mV**
f-FLBP_DMF-T	3.82	0.20	3.25	0.24	91	12
f-FLBP_tol-T	1.08	0.07	0.69	0.07	154	13
f-FLBP_DMF_MW	4.07	0.20	1.69	0.30	134	16
f-FLBP_tol_MW	2.58	0.09	2.45	0.08	147	8
FLBP_DMF	1.93	0.09	1.31	0.10	182	12

FLBP_tol	-	-	-	-	-	-

The highest current density of the anodic and cathodic peak, and the lowest peak to peak separation of f-FLBP_DMF-T could be attributed to the functionalised surface with the lowest resistance. It is correlated with the rate of functionalisation and additional phosphorus-nitrogen functional groups from the reaction of FLBP with 4-azidobenzoic acid at 140 °C, DMF decomposition products, and the amount of hydroxyl groups derived from the partial oxidation of FLBP. Both f-FLBP_tol-T and f-FLBP_tol-MW are marked by a similar ΔE at about 150 mV, but f-FLBP_tol-T demonstrates lower current densities of oxidation and reduction peaks than f-FLBP_tol-MW (Table 2). This is related to the higher resistance of obtained f-FLBP_tol-T and more sluggish charge transfer than f-FLBP_tol-MW. This indicate smaller functionalised electrochemically active area of the f-FLBP_tol-T surface [61]. The high degree of coverage of f-FLBP_tol-MW was confirmed by absent of phosphorus in the XPS spectrum. However, it should be noted for f-FLBP_tol-MW that both the cathodic and anodic peak currents are comparable.

To sum up, the f-FLBP with the comparable peaks of oxidation and reduction reaction was obtained by the synthesis in a microwave reactor in a toluene solution. This is due to the minor incidence of impurities generated during the preparation of the f-FLBP. However, the highest current densities of the electrode material and the smallest of the peak-to-peak separation is related to a lowest resistance of functionalised material and fast electron transfer during oxidation and reduction reactions recorded for the f-FLBP_DMF-T electrode [31]. Thus, the f-FLBP_DMF-T electrode was chosen for biosensing application.

5. *Haemophilus Influenzae* bacterial protein detection using antibody-modified f-FLBP_DMF-T

5.1 f-FLBP_DMF-T electrode modification

In Figure 10, the scheme of modification of a f-FLBP electrode for the detection of *Haemophilus Influenzae* bacterial protein is shown. The GC electrode (Φ 3 mm) with the f-FLBP_DMF-T layer was gently washed with demineralised water and then dried before the preparation of the electrode for the detection process. In the next step, the electrodes were tested using an appropriate procedure to determine the formal oxidation charge of ferrocyanides, and their impedance spectrum was recorded. Then, 40 μL of EDC, NHS and antibody containing solution was dropped on the electrode surface. This solution was obtained by mixing 20.9 mg NHS with 34.5 mg EDC in 5 ml PBS, then 1 mL of this solution was mixed with 40 μL of diluted antibodies (1:999), and the whole was deoxygenated. The electrolyte electrode was left for 24 hours in a vessel filled with argon at 4 ^{o}C. After this time, the electrode was washed with demineralised water. The next step of the electrode preparation for bacteria detection was incubation in a 0.01% solution of BSA in PBS for an hour, in an argon-filled vessel at 4 ^{o}C.

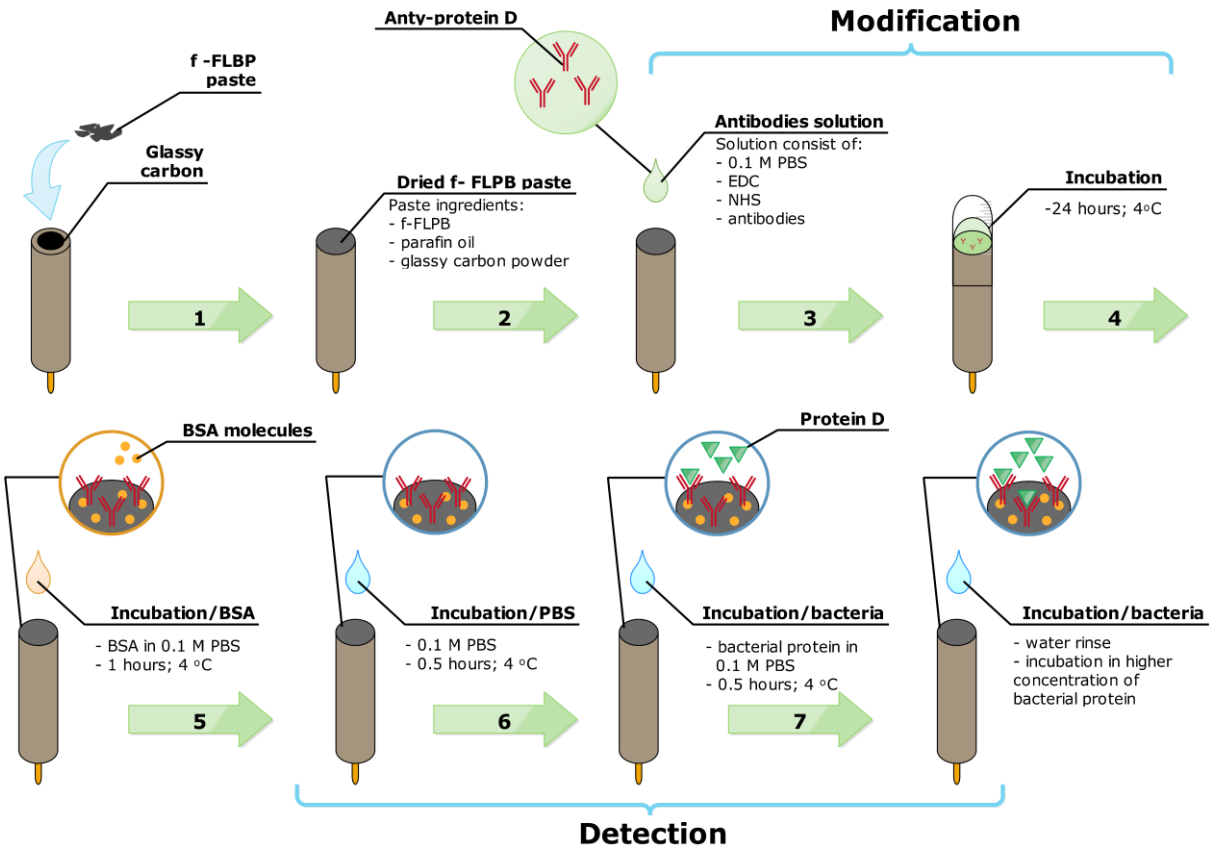

Figure 10. The modification of f-FLBP **(modification)** and incubation in bacterial protein as a part of detection **(detection).**

At each stage of modification, the sample was examined by means of cyclic voltammetry (CV) and electrochemical impedance spectroscopy (EIS). The measurements were carried out in 200 µL previously deoxygenated with an argon stream of a solution of 1 mM $K_3[Fe(CN)_6]$ in PBS at 7.4 pH. The measuring system consisted of three electrodes: a reference silver chloride electrode, a platinum mesh as a counter-electrode, and a working electrode, i.e. a GC electrode with f-FLBP_DMF-T. The electrochemical tests during modification of f-FLBP_DMF-T and detection of *Haemophilus Influenzae* bacterial protein were investigated using a potentiostat-galvanostat (VMP-300, Bio-Logic, France). CV was performed for each prepared electrode to determine the formal $Fe(CN)_6^{-3/-4}$ oxidation potential. The measurement was performed in the range from -0.75 V to + 0.75 V relative to the reference electrode at a speed of 50 mV s^{-1}. Then, EIS was performed around the previously determined formal

potential of ferrocyanide oxidation in the frequency range from 0.2 Hz – 10 kHz with single sine wave excitation with an amplitude of 10 mV. The sample polarisation time was 3 minutes. The impedance spectra of samples in various forms and the dependence of the current on the voltage flowing through the sample at various stages of modification are shown in Figure 11.

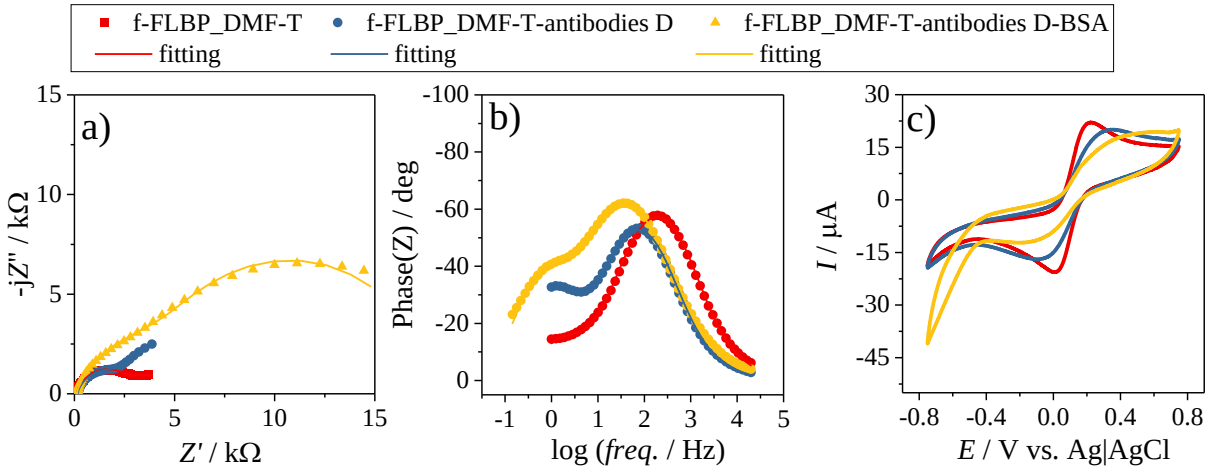

Figure 11. Modification of f-FLBP_DMF-T electrode: (A) registered EIS in Nyquist representation, (B) registered EIS in Bode representation, (C) registered CV. Recorded in 1 mM $K_3[Fe(CN)_6]$ in PBS at 7.4 pH.

Both the EIS spectrum in Nyquist's and Bode representation show two time constants arising after the incubation stage of the sample in the solution containing the antibodies, which may indicate the formation of two areas — the modified one, where the surface-bound antibody and the unmodified one occur. To analyse the obtained data, the circuit shown in Figure S5 was selected, which contains two time constants. The values obtained in this way are shown as the average of all collected samples along with the error expressed as standard deviation (S) in Table 3. The value of R_1 was omitted as a constant and was approximately 150 Ohm.

Table 3. Values of electric elements calculated for electric equivalent circuits registered during the electrode modification of f-FLBP_DMF-T

	Q_2/ μF $s^{(n-1)}$	±S μF $s^{(n-1)}$	n -	±S -	R_2/ kΩ	±S kΩ	R_3/ kΩ	±S kΩ	C_3/ μF	±S μF
f-FLBP_DMF-T	5.15	0.01	0.81	0.14	9.68	11.04	1.31	1.31	82.65	56.24
f-FLBP_DMF-T -antiprotein D	38.45	52.52	0.68	0.08	9.11	4.17	2.07	2.70	166.07	176.70
f-FLBP_DMF-T -antiprotein D - BSA	27.24	15.18	0.74	0.02	16.08	2.30	2.10	2.10	14.85	5.60

Analysis of the obtained data shows that the surface containing the antibodies is probably represented by the first part of the equivalent circuit (CPE /R_2) as indicated by the increase in resistance after 24 h incubation of the sample in the antibodies. However, the value of R_3 resistance at this stage decreased, which may be associated with partial phosphorus degradation in a humid environment [12,67,68]. After the next stage of sample modification with BSA, we can observe a further increase in R_2 and R_3 resistance as well as a decrease in Q_2 (CPE) and C_3 capacity, which is caused by the adsorption of BSA molecules on the surface — both in places where antibodies occur and on the unmodified surface. It is also worth noting the increase of the parameter *n* determining the degree of uniformity of the surface, which also confirms the adsorption of BSA. The current dependence on the voltage applied to the sample (Figure 11c) shows well the correlated changes with the EIS — the decrease in peak height is caused by the increase in sample resistance.

5.2 Detection of Haemophilus Influenzae bacterial protein

The detection of *Haemophilus Influenzae* was carried out by the electrochemical impedance spectroscopy (EIS) method. After completing the modification of the f-FLBP_DMF-T electrode, 40 µl of deoxygenated PBS solution (pH ≈ 7) was left on its surface for 30 minutes at 4 °C to determine the stability of the sensor surface, and thus estimating its blank response. The electrode was then washed gently with demineralised water and dried to perform an EIS measurement according to the modification procedure. Figure 12 presents the EIS spectra and CV of the modified f-FLBP_DMF-T for increased concentrations of *Haemophilus Influenzae* bacterial protein.

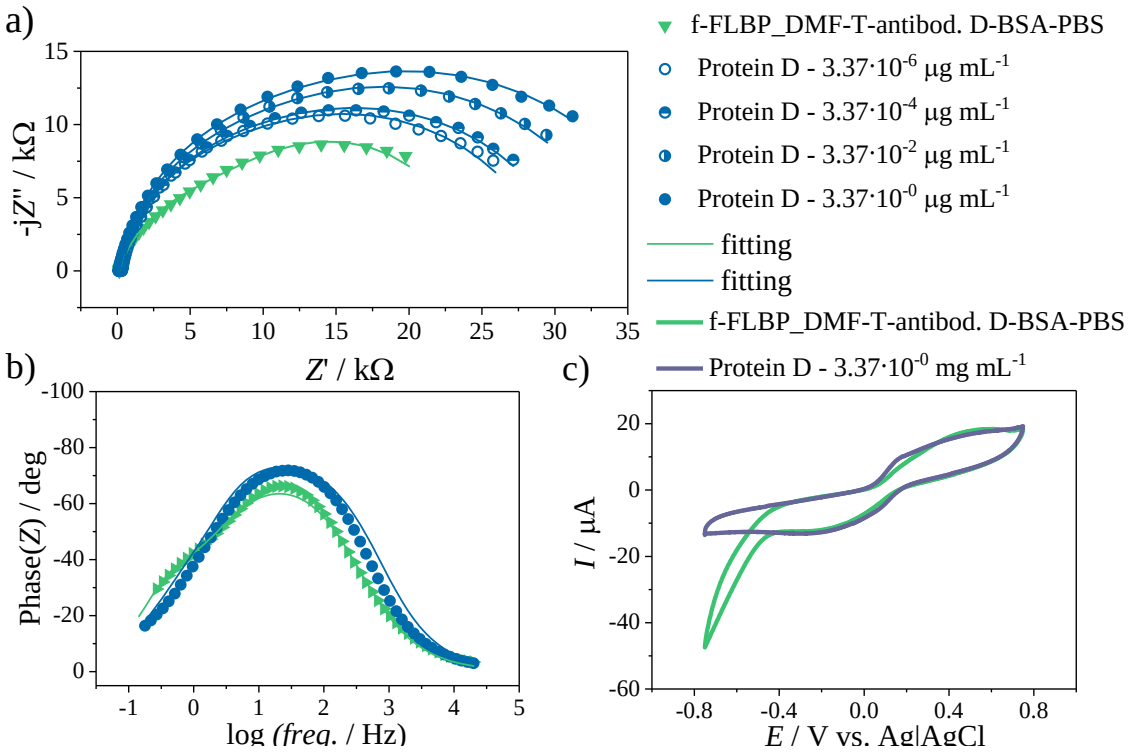

Figure 12. Detection of *Haemophilus Influenzae* protein D using modified f-FLBP_DMF-T: a) registered EIS in Nyquist representation, b) registered EIS in Bode representation, c) registered CV. Recorded in 1 mM $K_3[Fe(CN)_6]$ in PBS at 7.4 pH

The recorded impedance spectra were approximated using an elaborated equivalent electric circuit (EQEC). Circuit elements represent retrospective phenomena occurred at the sensing electrode. The estimated values with S of the EQEC elements are listed in Table 4.

Table 4. Values of EQEC elements estimated for modified f-FLBP_DMF-T recorded during *Haemophilus*

	Q_2 / $\mu F\ s^{(n-1)}$	±S $\mu F\ s^{(n-1)}$	n -	±S -	R_2 / kΩ	±S kΩ	R_3 / kΩ	±S kΩ	C_3 / µF	±S µF
PBS	17.03	8.31	0.76	0.01	22.38	4.28	3.79	3.54	33.33	22.88
Protein D 10E-6	13.95	2.67	0.79	0.02	25.75	5.33	7.21	2.36	12.19	0.95
Protein D 10E-4	12.29	5.54	0.79	0.02	28.27	5.78	6.71	3.80	13.45	2.03
Protein D 10E-2	12.63	2.60	0.81	0.01	30.16	6.07	7.37	3.39	13.48	0.60
Protein D 10E-0	9.36	3.93	0.84	0.03	32.29	6.31	8.67	2.53	33.03	27.72

Influenzae protein D detection.

The obtained changes of the R_2 resistance value were associated with the variation in protein D concentration, and a calibration curve was obtained with error bars expressed as the standard deviation of all relative change in R_2 resistance values for a given concentration (Fig.13). The relative change in R_2 resistance is shown as ΔR, which can be represented by equation (2) [69]:

$$\Delta R = \frac{R_{2_{PProtein}} - R_{2_{PBS}}}{R_{2_{PBS}}} \cdot 100\% \quad (2)$$

where:

ΔR – relative change of R_2; R_{2PBS} – resistance R_2 after incubation in PBS solution; and $R_{2Protein}$ – resistance R_2 after incubation in solution with protein.

The values exhibited in Figure 13 show that the charge transfer resistance value increased by (12.85±1.98)%, (20.65±1.27)%, (25.68±1.49)% and (30.63±1.15)% after incubation in $3.37 \cdot 10^{-6}$ µg mL^{-1}, $3.37 \cdot 10^{-4}$ µg mL^{-1}, $3.37 \cdot 10^{-2}$ µg mL^{-1}, and $3.37 \cdot 10^{0}$ µg mL^{-1} protein concentration, respectively. The limit of detection (LOD) is the lowest quantity of a substance that can be distinguished from the absence of that substance. In the case when the observed relationship to the analyte concentration is logarithmic, the LOD should be calculated by transforming the logarithmic relation, as Hao introduced in his work [70]. In our study, we used Equation 3:

$$x_D = ts_x = \frac{t}{b} e^{\frac{y_0 - a}{b}} \left[s_y^2 + s_a^2 + \left(\frac{y_0 - a}{b} \right)^2 s_b^2 \right]^{0.5} \quad (3)$$

Where s_b, s_a, s_x, and s_y are the deviation of the slope, intercept, concentration, and response signal, respectively. Confidence factor t = 3 was selected.

The limit of detection achieved was **5.82 µg mL^{-1}**, while the *Haemophilus Influenzae* bacterial protein determination sensitivity was equal to **1.2763%µg^{-1} mL**. The developed electrochemical biosensor displayed a wide linear range from $3.37 \cdot 10^{-6}$ to 3.37 µg mL^{-1} for the determination of *Haemophilus Influenzae* bacterial protein. The logarithmic scale allows numerical data over a very wide range of values to be viewed [71], where the relative change of resistance of the modified f-FLBP_DMF-T electrode *vs.* the exponential growth of the concentration of the bacterial protein takes place. It should be noted that the wide detection range of bacterial protein concentration allows the method to be used for real samples, where the concentration is not specified and in a wide range.

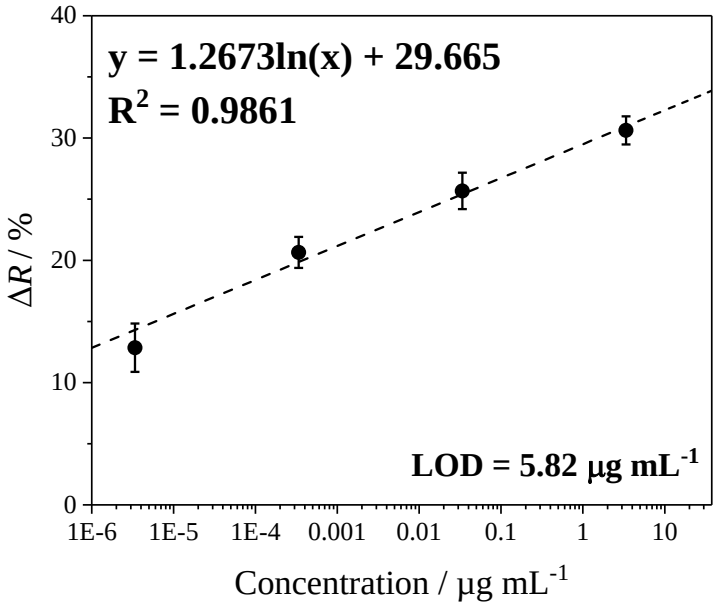

Figure 13. The relation between the relative change of resistance of modified f-FLBP_DMF-T after incubation in different concentrations of *Haemophilus Influenzae* bacterial protein and concentration of bacterial protein solution on a logarithmic scale.

6 Conclusion

In summary, four strategies of functionalisation of few-layer black phosphorus by 4-azidobenzoic acid were studied in detail.: functionalised few-layer black phosphorus obtained at 140 °C in DMF (f-FLBP_DMF-T) or in toluene (f-FLBP_tol-T) as a solvent, and functionalised few-layer black phosphorus produced at 70 °C in a microwave reactor using DMF (f-FLBP_DMF-MW) or toluene (f-FLBP_tol-MW) as a medium of reaction. Electrochemical tests of the f-FLBP_tol-MW exhibited highly reversibility of reactions using a ferricyanide/ferrocyanide redox probe. The highest current densities of oxidation and reduction peaks, and the lowest peak-to-peak separation values in 5 mM $K_3[Fe(CN)_6]$ /0.5M Na_2SO_4 solution, leading to better sensing properties, were obtained for the f-FLBP_DMF-T. The biosensing application of the f-FLBP_DMF-T electrode was successfully demonstrated by detection of the *Haemophilus Influenzae* bacterial protein. The impedance technique was

employed to determine the concentration of bacterial protein, revealing as low a limit of detection as 5.82 μg mL^{-1}, and a sensitivity equal to 1.267 % μg^{-1} mL. Other methods, such as PCR (polymerase chain reaction), have a lower LOD of $2.5 \cdot 10^3$ genome copies per millilitre [72] to $1.89 \cdot 10^6$ copies per millilitre [73], but take more time [74]. Real-time PCR is faster [75] than conventional culturing and identification, but the impedimetric method used in our work using functionalised few-layer black phosphorus as a biosensing platform is much faster (one and half hours) and can potentially lead to exciting opportunities for use to build portable devices for rapid detection of *Haemophilus Influenzae* bacteria.Thus, f-FLBP_DMF-T may be an attractive and alternative novel electrode material for the sensitive detection of various bacterial pathogens.

Acknowledgements

This work was supported by the Polish National Science Centre [2016/22/E/ST7/00102]; and the National Centre for Science and Development [347324/12/NCBR/2017]. The DS funds of the Faculty of Electronics, Telecommunications and Informatics of the Gdansk University of Technology are also acknowledged.

References

[1] X. Ge, Z. Xia, S. Guo, Recent Advances on Black Phosphorus for Biomedicine and Biosensing, Adv. Funct. Mater. 29 (2019) 1–32. doi:10.1002/adfm.201900318.

[2] Y. Yi, X. Yu, W. Zhou, J. Wang, P.K. Chu, Two-dimensional black phosphorus : Synthesis , modi fi cation , properties , and applications, 120 (2017) 1–33. doi:10.1016/j.mser.2017.08.001.

[3] V. Eswaraiah, Q. Zeng, Y. Long, Z. Liu, Black Phosphorus Nanosheets: Synthesis, Characterization and Applications, Small. (2016) 3480–3502. doi:10.1002/smll.201600032.

[4] J. Miao, L. Zhang, C. Wang, Black phosphorus electronic and optoelectronic devices, 2D Mater. 6

(2019) ab1ebd. doi:10.1088/2053-1583/ab1ebd.

[5] P. Chen, N. Li, X. Chen, W.J. Ong, X. Zhao, The rising star of 2D black phosphorus beyond graphene: Synthesis, properties and electronic applications, 2D Mater. 5 (2018). doi:10.1088/2053-1583/aa8d37.

[6] F. Xu, B. Ge, J. Chen, A. Nathan, L.L. Xin, H. Ma, H. Min, C. Zhu, W. Xia, Z. Li, S. Li, K. Yu, L. Wu, Y. Cui, L. Sun, Y. Zhu, Scalable shear-exfoliation of high-quality phosphorene nanoflakes with reliable electrochemical cycleability in nano batteries, 2D Mater. (2016). doi:10.1088/2053-1583/3/2/025005.

[7] J.O. Island, G.A. Steele, H.S.J. Van Der Zant, A. Castellanos-Gomez, Environmental instability of few-layer black phosphorus, 2D Mater. 2 (2015). doi:10.1088/2053-1583/2/1/011002.

[8] G. Wang, W.J. Slough, R. Pandey, S.P. Karna, Degradation of phosphorene in air: Understanding at atomic level, 2D Mater. 3 (2016) 1–7. doi:10.1088/2053-1583/3/2/025011.

[9] Y. Wang, B. Yang, B. Wan, X. Xi, Z. Zeng, E. Liu, G. Wu, Z. Liu, W. Wang, Degradation of black phosphorus: A real-time31P NMR study, 2D Mater. 3 (2016). doi:10.1088/2053-1583/3/3/035025.

[10] A. Dettlaff, G. Skowierzak, Ł. Macewicz, M. Sobaszek, J. Karczewski, M. Sawczak, J. Ryl, T. Ossowski, R. Bogdanowicz, Electrochemical Stability of Few-Layer Phosphorene Flakes on the Boron-Doped Diamond: Wide Potential Range Studies in Aqueous Solvents, J. Phys. Chem. C. 123 (2019) 20233–20240. doi:10.1021/acs.jpcc.9b03028.

[11] A.E. Del Río Castillo, C.D. Reyes-Vazquez, L.E. Rojas-Martinez, S.B. Thorat, M. Serri, A.L. Martinez-Hernandez, C. Velasco-Santos, V. Pellegrini, F. Bonaccorso, Single-step exfoliation and functionalization of few-layers black phosphorus and its application for polymer composites, FlatChem. 18 (2019) 100131. doi:10.1016/j.flatc.2019.100131.

[12] R. Jain, Y. Singh, S.Y. Cho, S.P. Sasikala, S.H. Koo, R. Narayan, H.T. Jung, Y. Jung, S.O. Kim, Ambient Stabilization of Few Layer Phosphorene via Noncovalent Functionalization with Surfactants: Systematic 2D NMR Characterization in Aqueous Dispersion, Chem. Mater. 31 (2019) 2786–2794. doi:10.1021/acs.chemmater.8b04984.

[13] R. Guo, Y. Zheng, Z. Ma, X. Lian, H. Sun, C. Han, H. Ding, Q. Xu, X. Yu, J. Zhu, W. Chen, Surface passivation of black phosphorus via van der Waals stacked PTCDA, Appl. Surf. Sci. 496 (2019) 143688. doi:10.1016/j.apsusc.2019.143688.

[14] G. Tiouitchi, M. Raji, O. Mounkachi, M.A. Ali, A. Mahmoud, F. Boschini, H. Essabir, R. Bouhfid, A. el kacem Qaiss, Black phosphorus-based polyvinylidene fluoride nanocomposites: Synthesis, processing and characterization, Compos. Part B Eng. 175 (2019) 107165. doi:10.1016/j.compositesb.2019.107165.

[15] W. Liu, Y. Zhu, S. Wang, X. Ban, X. Xu, X. Zhang, Effective improvement in capacitance performance of polypyrrole assisted by black phosphorus, J. Mater. Sci. Mater. Electron. 30 (2019) 15130–15138. doi:10.1007/s10854-019-01885-x.

[16] X. Li, X. Niu, W. Zhao, W. Chen, C. Yin, Y. Men, G. Li, W. Sun, Black phosphorene and PEDOT:PSS-modified electrode for electrochemistry of hemoglobin, Electrochem. Commun. 86 (2018) 68–71. doi:10.1016/j.elecom.2017.11.017.

[17] J. Cai, X. Gou, B. Sun, W. Li, D. Li, J. Liu, F. Hu, Y. Li, Porous graphene-black phosphorus nanocomposite modified electrode for detection of leptin, Biosens. Bioelectron. 137 (2019) 88–95. doi:10.1016/j.bios.2019.04.045.

[18] Y. Cai, S. Li, Y. Zhou, K. Da Xu, Y. Wang, S. Zuo, W. Joines, Investigation of multi-resonant and anisotropic plasmonic resonances in the stacked graphene-black phosphorus bilayers, J. Phys. D. Appl. Phys. 53 (2020) ab4eea. doi:10.1088/1361-6463/ab4eea.

[19] Q.X. Pei, X. Zhang, Z. Ding, Y.W.Y.Y. Zhang, Y.W.Y.Y. Zhang, Thermal stability and thermal conductivity of phosphorene in phosphorene/graphene van der Waals heterostructures, Phys. Chem. Chem. Phys. 19 (2017) 17180–17186. doi:10.1039/c7cp02553j.

[20] J. Zhu, A.N. Gandi, M. Gu, B- Doping- Enhanced Stability of Phosphorene/Graphene Heterostructures, Adv. Theory Simulations. 2 (2019) 1800176. doi:10.1002/adts.201800176.

[21] X.Q. Tian, X.R. Wang, Y.D. Wei, L. Liu, Z.R. Gong, J. Gu, Y. Du, B.I. Yakobson, Highly Tunable Electronic Structures of Phosphorene/Carbon Nanotube Heterostructures through External Electric Field and Atomic Intercalation, Nano Lett. 17 (2017) 7995–8004. doi:10.1021/acs.nanolett.7b04562.

[22] H. Li, P. Lian, Q. Lu, J. Chen, R. Hou, Y. Mei, Excellent air and water stability of two-dimensional black phosphorene/MXene heterostructure, Mater. Res. Express. 6 (2019) 65504. doi:10.1088/2053-1591/ab0b84.

[23] R. Zhao, Z. Qian, Z. Liu, D. Zhao, X. Hui, G. Jiang, C. Wang, L. Yin, Molecular-level heterostructures

assembled from layered black phosphorene and Ti3C2 MXene as superior anodes for high-performance sodium ion batteries, Nano Energy. 65 (2019) 104037. doi:10.1016/j.nanoen.2019.104037.

[24] C.R. Ryder, J.D. Wood, S.A. Wells, Y. Yang, D. Jariwala, T.J. Marks, G.C. Schatz, M.C. Hersam, Covalent functionalization and passivation of exfoliated black phosphorus via aryl diazonium chemistry, Nat. Chem. 8 (2016) 597–602. doi:10.1038/nchem.2505.

[25] Z. Sofer, J. Luxa, D. Bouša, D. Sedmidubský, P. Lazar, T. Hartman, H. Hardtdegen, M. Pumera, The Covalent Functionalization of Layered Black Phosphorus by Nucleophilic Reagents, Angew. Chemie - Int. Ed. 56 (2017) 9891–9896. doi:10.1002/anie.201705722.

[26] Y. Liu, P. Gao, T. Zhang, X. Zhu, M. Zhang, M. Chen, P. Du, G.W. Wang, H. Ji, J. Yang, S. Yang, Azide Passivation of Black Phosphorus Nanosheets: Covalent Functionalization Affords Ambient Stability Enhancement, Angew. Chemie - Int. Ed. 58 (2019) 1479–1483. doi:10.1002/anie.201813218.

[27] J.M. Marmolejo-Tejada, A. Jaramillo-Botero, Partially-oxidized phosphorene sensor for the detection of sub-nano molar concentrations of nitric oxide: A first-principles study, Phys. Chem. Chem. Phys. 21 (2019) 19083–19091. doi:10.1039/c9cp03912k.

[28] P. Rubio-Pereda, G. H. Cocoletzi, Density functional theory calculations of biomolecules adsorption on phosphorene for biomedical applications, Appl. Surf. Sci. 427 (2018) 1227–1234. doi:10.1016/j.apsusc.2017.08.198.

[29] M. Jakhar, A. Kumar, S. Srivastava, P. Parida, K. Tankeshwar, Adsorption of nucleobases on different allotropes of phosphorene, AIP Conf. Proc. 2115 (2019). doi:10.1063/1.5113200.

[30] Y. Zhao, Y.-H. Zhang, Z. Zhuge, Y.-H. Tang, J.-W. Tao, Y. Chen, Synthesis of a Poly-L-lysine/Black Phosphorus Hybrid for Biosensors, Anal. Chem. (2018) acs.analchem.7b04395. doi:10.1021/acs.analchem.7b04395.

[31] Y. Ge, M.B. Camarada, L. Xu, M. Qu, H. Liang, E. Zhao, M. Li, Y. Wen, A highly stable black phosphorene nanocomposite for voltammetric detection of clenbuterol, Microchim. Acta. 185 (2018) 566. doi:10.1007/s00604-018-3084-z.

[32] Z. Zhang, Y. Li, J. Xu, Y. Wen, Electropolymerized molecularly imprinted polypyrrole decorated with black phosphorene quantum dots onto poly(3,4-ethylenedioxythiophene) nanorods and its voltammetric

sensing of vitamin C, J. Electroanal. Chem. 814 (2018) 153–160. doi:10.1016/j.jelechem.2018.02.059.

[33] Y. Ge, M. Qu, L. Xu, X. Wang, J. Xin, X. Liao, M.M. Li, M.M. Li, Y. Wen, Phosphorene nanocomposite with high environmental stability and antifouling capability for simultaneous sensing of clenbuterol and ractopamine, Microchim. Acta. 186 (2019). doi:10.1007/s00604-019-3908-5.

[34] S. Liang, L. Wu, H. Liu, J. Li, M. Chen, M. Zhang, Organic molecular passivation of phosphorene: An aptamer-based biosensing platform, Biosens. Bioelectron. 126 (2019) 30–35. doi:10.1016/j.bios.2018.10.037.

[35] A. Kumar, Simultaneous Passivation and Encapsulation of Black Phosphorus Nanosheets (Phosphorene) by Optically Active Polypeptide Micelles for Biosensors, ACS Appl. Nano Mater. 2 (2019) 2397–2404. doi:10.1021/acsanm.9b00265.

[36] Y. Liu, P. Gao, T. Zhang, X. Zhu, M. Zhang, M. Chen, P. Du, G.W. Wang, H. Ji, J. Yang, S. Yang, Azide Passivation of Black Phosphorus Nanosheets: Covalent Functionalization Affords Ambient Stability Enhancement, Angew. Chemie - Int. Ed. 58 (2019) 1479–1483. doi:10.1002/anie.201813218.

[37] QuantumATK, Synopsys QuantumATK, QuantumATK O-2018.06, (n.d.).

[38] S. Smidstrup, T. Markussen, P. Vancraeyveld, J. Wellendorff, J. Schneider, T. Gunst, B. Verstichel, D. Stradi, P.A. Khomyakov, U.G. Vej-Hansen, M.E. Lee, S.T. Chill, F. Rasmussen, G. Penazzi, F. Corsetti, A. Ojanperä, K. Jensen, M.L.N. Palsgaard, U. Martinez, A. Blom, M. Brandbyge, K. Stokbro, QuantumATK: An integrated platform of electronic and atomic-scale modelling tools, J. Phys. Condens. Matter. 32 (2020). doi:10.1088/1361-648X/ab4007.

[39] S. Smidstrup, D. Stradi, J. Wellendorff, P.A. Khomyakov, U.G. Vej-Hansen, M.E. Lee, T. Ghosh, E. Jónsson, H. Jónsson, K. Stokbro, First-principles Green's-function method for surface calculations: A pseudopotential localized basis set approach, Phys. Rev. B. 96 (2017) 1–17. doi:10.1103/PhysRevB.96.195309.

[40] V. Nagarajan, R. Chandiramouli, Interaction of volatile organic compounds (VOCs) emitted from banana on stanene nanosheet—a first-principles studies, Struct. Chem. 29 (2018) 1321–1332. doi:10.1007/s11224-018-1114-4.

[41] R. Chandiramouli, Antimonene nanosheet device for detection of explosive vapors – A first-principles

inspection, Chem. Phys. Lett. 708 (2018) 130–137. doi:10.1016/j.cplett.2018.08.016.

[42] U. Srimathi, V. Nagarajan, R. Chandiramouli, Germanane nanosheet as a novel biosensor for liver cirrhosis based on adsorption of biomarker volatiles – A DFT study, Appl. Surf. Sci. 475 (2019) 990–998. doi:10.1016/j.apsusc.2019.01.008.

[43] N. Rani, J.P. Shrivastava, R.K. Bajpai, Deccan traps-associated obsidian glass: A nuclear waste containment, Curr. Sci. 105 (2013) 371–378.

[44] B. Viswanathan, S. Murugesan, A. Ariharan, K.S. Lakhi, Hetero Atom Substituted Carbon—Potential Hydrogen Storage Materials, Adv. Porous Mater. 1 (2013) 122–128. doi:10.1166/apm.2013.1008.

[45] E. Lieber, C.N.R.N.R. Rao, A.E.E. Thomas, E. Oftedahl, R. Minnis, C.V.N.V.N. Nambury, Infrared spectra of acid azides, carbamyl azides and other azido derivatives. Anomalous splittings of the N3 stretching bands, Spectrochim. Acta. 19 (1963) 1135–1144. doi:10.1016/0371-1951(63)80033-8.

[46] B.H. Stuart, Infrered Spectroscopy: Fundamentals and Applications, John Wiley & Sons, Ltd, 2004.

[47] M. Bolboaca, T. Stey, A. Murso, D. Stalke, W. Kiefer, P-N bond length alterations monitored by infrared absorption and Fourier transform Raman spectroscopy in combination with density functional theory calculations, Appl. Spectrosc. 57 (2003) 970–976. doi:10.1366/000370203322258931.

[48] McMurry John, Organic Chemistry, 9th ed., 2015.

[49] D. Gupta, D. Jamwal, D. Rana, A. Katoch, Microwave synthesized nanocomposites for enhancing oral bioavailability of drugs, Elsevier Inc., 2018. doi:10.1016/b978-0-12-813741-3.00027-3.

[50] K. Zhang, B. Jin, C. Park, Y. Cho, X. Song, X. Shi, S. Zhang, W. Kim, H. Zeng, J.H. Park, Black phosphorene as a hole extraction layer boosting solar water splitting of oxygen evolution catalysts, Nat. Commun. 10 (2019) 1–10. doi:10.1038/s41467-019-10034-1.

[51] and S.Y. Yajuan Liu, Pengfei Gao, Taiming Zhang, Xianjun Zhu, Mengmeng Zhang, Muqing Chen, Pingwu Du, Guan-Wu Wang, Hengxing Ji,* Jinlong Yang, Azide passivation of Black Phosphorus Nanosheets: Covalent Functionalization Affords Ambient Stability Enhancement, Angew. Chemie - Int. Ed. 50 (2018) 1479–1483. doi:10.1002/anie.201813218.

[52] D. Banerjee, K.J. Sankaran, S. Deshmukh, M. Ficek, G. Bhattacharya, J. Ryl, D.M. Phase, M. Gupta, R. Bogdanowicz, I.N. Lin, A. Kanjilal, K. Haenen, S.S. Roy, 3D Hierarchical Boron-Doped Diamond-

Multilayered Graphene Nanowalls as an Efficient Supercapacitor Electrode, J. Phys. Chem. C. 123 (2019) 15458–15466. doi:10.1021/acs.jpcc.9b03628.

[53] L. Wang, Z. Sofer, M. Pumera, Voltammetry of Layered Black Phosphorus: Electrochemistry of Multilayer Phosphorene, ChemElectroChem. 2 (2015) 324–327. doi:10.1002/celc.201402363.

[54] A. Dettlaff, G. Skowierzak, Ł. Macewicz, M. Sobaszek, J. Karczewski, M. Sawczak, J. Ryl, T. Ossowski, R. Bogdanowicz, Electrochemical Stability of Few-Layered Phosphorene Flakes on Boron-Doped Diamond: A Wide Potential Range of Studies in Aqueous Solutions, J. Phys. Chem. C. 123 (2019) 20233–20240. doi:10.1021/acs.jpcc.9b03028.

[55] Y. Wang, A. Slassi, J. Cornil, D. Beljonne, P. Samorì, Tuning the Optical and Electrical Properties of Few-Layer Black Phosphorus via Physisorption of Small Solvent Molecules, Small. 15 (2019) 1–8. doi:10.1002/smll.201903432.

[56] M. Schock, S. Bräse, Reactive & efficient: Organic azides as cross-linkers in material sciences, Molecules. 25 (2020). doi:10.3390/molecules25041009.

[57] H.R. Allcock, Phosphorus-nitrogen compounds, Academic Press, New York and London, 1972.

[58] J. Muzart, N,N-Dimethylformamide: much more than a solvent, Tetrahedron. 65 (2009) 8313–8323. doi:10.1016/j.tet.2009.06.091.

[59] D. Plana, R.A.W. Dryfe, The electro-oxidation of dimethylamine borane: Part 1, polycrystalline substrates, Electrochim. Acta. 56 (2011) 3835–3844. doi:10.1016/j.electacta.2011.02.041.

[60] S. Ramalingam, R. Chand, C.B. Singh, A. Singh, Phosphorene-gold nanocomposite based microfluidic aptasensor for the detection of okadaic acid, Biosens. Bioelectron. 135 (2019) 14–21. doi:10.1016/j.bios.2019.03.056.

[61] X. Li, G. Luo, H. Xie, Y. Niu, X. Li, R. Zou, Y. Xi, Y. Xiong, W. Sun, G. Li, Voltammetric sensing performances of a carbon ionic liquid electrode modified with black phosphorene and hemin, Microchim. Acta. 186 (2019). doi:10.1007/s00604-019-3421-x.

[62] R.S. Nicholson, I. Shain, Theory of Stationary Electrode Polarography for a Chemical Reaction Coupled between Two Charge Transfers, Anal. Chem. 37 (1965) 178–190. doi:10.1021/ac60221a002.

[63] Y. Xiang, M.B. Camarada, Y. Wen, H. Wu, J. Chen, M. Li, X. Liao, Simple voltammetric analyses of

ochratoxin A in food samples using highly-stable and anti-fouling black phosphorene nanosensor, Electrochim. Acta. 282 (2018) 490–498. doi:10.1016/j.electacta.2018.06.055.

[64] R. Trouillon, D. O'Hare, Comparison of glassy carbon and boron doped diamond electrodes: Resistance to biofouling, Electrochim. Acta. 55 (2010) 6586–6595. doi:10.1016/j.electacta.2010.06.016.

[65] R. Gusmão, Z. Sofer, D. Bouša, M. Pumera, Black Phosphorus Synthesis Path Strongly Influences Its Delamination, Chemical Properties and Electrochemical Performance, ACS Appl. Energy Mater. (2018). doi:10.1021/acsaem.7b00106.

[66] L. Lodovico, V.L. Martins, T.M. Benedetti, R.M. Torresi, Electrochemical behavior of iron and magnesium in ionic liquids, J. Braz. Chem. Soc. 25 (2014) 460–468. doi:10.5935/0103-5053.20130305.

[67] C. Hyun, J.H. Kim, J.Y. Lee, G.H. Lee, K.S. Kim, Atomic scale study of black phosphorus degradation, RSC Adv. 10 (2019) 350–355. doi:10.1039/c9ra08029e.

[68] C. Xing, J. Zhang, J. Jing, J. Li, F. Shi, Preparations, properties and applications of low-dimensional black phosphorus, Chem. Eng. J. 370 (2019) 120–135. doi:10.1016/j.cej.2019.03.177.

[69] 1-s2, (n.d.).

[70] P. Van Hao, C.T. Xuan, P.D. Thanh, N.T. Thuat, N.H. Hai, M.A. Tuan, Detection analysis limit of nonlinear characteristics of DNA sensors with the surface modified by polypyrrole nanowires and gold nanoparticles, J. Sci. Adv. Mater. Devices. 3 (2018) 129–138. doi:10.1016/j.jsamd.2018.04.002.

[71] H. Liang, H. Xu, Y. Zhao, J. Zheng, H. Zhao, G. Li, C.P. Li, Ultrasensitive electrochemical sensor for prostate specific antigen detection with a phosphorene platform and magnetic covalent organic framework signal amplifier, Biosens. Bioelectron. 144 (2019) 111691. doi:10.1016/j.bios.2019.111691.

[72] K.M. Hare, R.L. Marsh, M.J. Binks, K. Grimwood, S.J. Pizzutto, A.J. Leach, A.B. Chang, H.C. Smith-Vaughan, Quantitative PCR confirms culture as the gold standard for detection of lower airway infection by nontypeable Haemophilus influenzae in Australian Indigenous children with bronchiectasis, J. Microbiol. Methods. 92 (2013) 270–272. doi:10.1016/j.mimet.2012.12.013.

[73] X. Fan, X. Liu, L. Ji, D. Cai, J. Jiang, J. Zhu, A. Sun, J. Yan, Epidemiological analysis and rapid detection by one-step multiplex PCR assay of Haemophilus influenzae in children with respiratory tract infections in Zhejiang Province, China, BMC Infect. Dis. 18 (2018) 1–6. doi:10.1186/s12879-018-3295-

[74] N. Ishiwada, L.D. Cao, Y. Kohno, PCR-based capsular serotype determination of Haemophilus influenzae strains recovered from Japanese paediatric patients with invasive infection, Clin. Microbiol. Infect. 10 (2004) 895–898. doi:10.1111/j.1469-0691.2004.00966.x.

[75] A. Marty, O. Greiner, P.J.R. Day, S. Gunziger, K. Mühlemann, D. Nadal, Detection of Haemophilus influenzae type b by real-time PCR, J. Clin. Microbiol. 42 (2004) 3813–3815. doi:10.1128/JCM.42.8.3813-3815.2004.